Journal of Geophysical Research: Planets

RESEARCH ARTICLE
10.1029/2018JE005613

Special Section:
5th International Planetary Dunes Workshop Special Issue

Dune Casts Preserved by Partial Burial: The First Identification of *Ghost Dune* Pits on Mars

Mackenzie D. Day[1] and **David C. Catling**[1]

[1]Department of Earth and Space Sciences and NASA Astrobiology Institute, University of Washington, Seattle, WA, USA

Key Points:
- Pits on Mars formed by removal of eolian dune sands after partial burial of the dunes
- Interdune deposits, possibly basaltic lava flows, were emplaced under low-energy conditions, causing minimal disruption to dune forms
- Pit morphology preserves a cast of the ancient flooded dune field

Correspondence to:
M. D. Day,
daym@uw.edu

Citation:
Day, M. D., & Catling, D. C. (2018). Dune casts preserved by partial burial: The first identification of *ghost dune* pits on Mars. *Journal of Geophysical Research: Planets*, *123*. https://doi.org/10.1029/2018JE005613

Received 16 MAR 2018
Accepted 17 MAY 2018
Accepted article online 5 JUN 2018

Abstract Eolian sediment transport is active on modern Mars and has been for billions of years. Dune fields dot the surface of the planet, and examples of preserved eolian strata confirm that dunes were active on ancient Mars. As is also true on Earth, most Martian eolian sandstones preserve only a small fraction of the strata that constituted ancient dunes, and whole dunes fields are rarely preserved. In this study, we focus on two fields of >300 pits each and compare the pit morphologies, scales, and orientations to modern Martian dunes. It is hypothesized that the pit fields studied in Noctis Labyrinthus and Hellas basin represent casts of dunes from two ancient dune fields that were partially buried in the Hesperian. The flood material concentrated in the interdune area then became indurated, while the loose eolian dune sands eroded away, leaving behind the ~10^2-m-scale dune-shaped pits or *ghost dune* pits. Modern barchan dunes in Oyama and Herschel craters are used for comparison to the pit fields, and the topography of these modern dunes is used to model pit morphologies after partial burial. Basalt flows and low-energy fluviolacustrine deposition are possible mechanisms for partial burial. The potential for eolian strata to be preserved within the pits at a once warm or water-rich interface makes the pits of interest for astrobiology. The inferred ancient dune fields record in their morphology a wind regime that differs from the modern and provide rare evidence of whole dune field preservation.

Plain Language Summary Ancient dunes in two places on Mars were partially buried and then eroded away, leaving behind dune-shaped pits that preserve information about the ancient environment. These pits may contain ancient dune sandstones around the edges of the pits and could be a good place to look for evidence of ancient life. The shapes of the pits also tell us how the winds behaved in the past.

1. Introduction

Eolian processes actively shape the surface of Mars through the interactions of wind, mobile sand, and exposed bedrock. Eolian erosion can carve centimeter-scale ventifacts (Bridges et al., 2014; Laity, 1994), meter-scale yardangs (Ward, 1979), and even kilometer-scale mounds (Day et al., 2016; Steele et al., 2018). Depositional processes create ripple and dune fields at all latitudes across the planet (Hayward et al., 2014; Lapotre et al., 2016). Dunes in particular are well studied on both Earth and Mars and record in their morphology information about the local winds and sediment state (Courrech du Pont et al., 2014; Kocurek & Lancaster, 1999; Rubin & Hunter, 1987). Eolian processes have been a significant contributor to Martian landscape evolution since the Noachian-Hesperian transition (Carr, 1982; Greeley et al., 2001), and by studying ancient dunes, we can make inferences about the similarities and differences between the modern and ancient Martian climates.

On Earth, evidence of ancient eolian dunes can be found in terrestrial sandstones as sets of cross strata from the bases of ancient lee faces (e.g., Bristow & Hill, 1998; Brookfield, 1977; Hunter, 1976). Eolian strata typically capture only the basal lee portion of the ancient dunes and are most commonly exposed in vertical section, making the plan view morphology of the dunes difficult to interpret. Even where outcrops are exposed in plan view (e.g., Brothers et al., 2016; Day & Kocurek, 2017), topographic variation on an outcrop surface can cut through eolian bed sets, obscuring the morphologies of any single bedform with the superimposed signatures of later dunes. Measuring the variability in stratal dip directions can help constrain the morphology of ancient dunes (e.g., Banham et al., 2018; Kocurek & Day, 2017), but such hand-sample-scale measurements are impracticable for large-scale application to Mars.

In one instance of exotic preservation on Earth, dune morphologies were preserved by the partial burial and later removal of dune sands. Ancient barchan and barchanoid dunes on the eastern Snake River Plain were

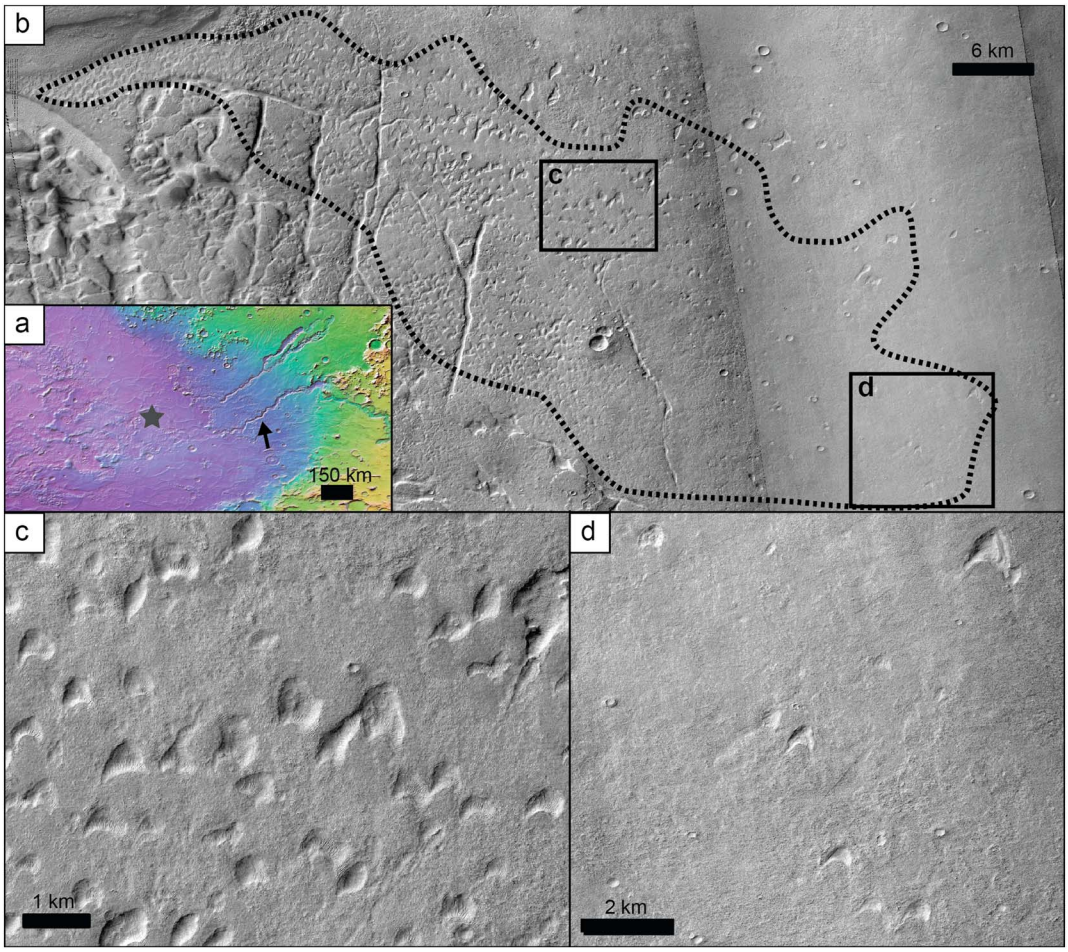

Figure 1. Dune cast pits in Hellas basin. (a) Location of the study area (black star) within Hellas basin to the southwest of several major fluvial channels. Mars Orbiter Laser Altimeter 128-ppd topography and Mars Viking global mosaic. Cool colors are low elevation and warm colors high. Total relief in this image is ~7 km. Two large fluvial channels dissect the eastern rim of the basin. Harmakhis Vallis to the south (arrow) and Dao Vallis to the north. (b) CTX mosaic showing the approximate extent of the pits interpreted to represent an ancient dune field (dotted line). The extent of (c) and (d) are shown in boxes. Mosaic of three CTX images: P16_007266_1392_XN_40S280W (right), P19_008558_1398_XI_40S281W (middle), and P19_008268_1392_XI_40S281W (left). (c) Barchanoid pits typical of the Hellas basin pit field. Note the concave-south shape of the majority of the pits, suggesting that these were south migrating dunes. (d) Barchan-shaped pits near the margin of the pit field showing clear classical barchan shape and consistently oriented to reflect southward migration. Sun is from the upper left. North is up in all figures. No High Resolution Imaging Science Experiment coverage was available for areas within the dotted line.

flooded by the Split Butte basalt flow (Gaylord et al., 2015; Kuntz et al., 1992), and later erosion of the dune sands left behind barchan-shaped pits in the basalt, termed *ghost dune* pits for their preservation of the dune morphology in negative topographic relief (Gaylord et al., 2016).

On Mars, the situation is much the same as on Earth. Preserved eolian strata have been identified by rovers (Banham et al., 2018; Grotzinger et al., 2005) and also by orbiters in both equatorial (Milliken et al., 2014) and polar latitudes (Brothers et al., 2018; Kocurek & Ewing, 2012). As with Earth, these deposits are dominantly cross sectional and preserve only basal dune strata in stacks of climbing sets. Rare instances of plan view outcrops preserve straight-crested (Bourke & Viles, 2016) and barchan dune morphologies (Schatz et al., 2006) but represent isolated instances preserving relatively recent dune forms. One extreme example of ancient preservation was identified in the Apollinaris Sulci region where an entire dune field appears to have been cemented and exhumed from under the retreating Medusa Fossae formation (Edgett & Blumberg, 1994; Edgett & Malin, 2000; Peterfreund, 1985). This exotic case represents the only documentation of ancient

dunes where the morphology of many dunes in the same field can be plainly observed. Although the morphology of any one dune captures some information, measuring many dunes in the same field increases the fidelity of interpretations made from the dune morphologies (Allen, 1976; Kocurek & Ewing, 2005).

In this work, we explore two locations on Mars where many dune morphologies are potentially preserved. Noctis Labyrinthus and Hellas basin both exhibit a series of pits in a local topographic low. Pitted terrains are common on Mars and have been attributed to a number of origins. However, to date no pits on Mars have been attributed to genesis by eolian dunes. We explore the possibility that pits in these two study sites on Mars are casts of ancient dunes, analogous to the ghost dunes of the eastern Snake River Plain, and discuss the implications of such an interpretation.

2. Study Areas and Geologic Context

2.1. Pit Field in Hellas Basin

We discuss two putative paleodune fields, the first of which lies near the eastern margin of Hellas basin. At the regional scale, eastern Hellas basin is highly fluvially dissected with major channel systems flowing from ENE to WSW (Crown et al., 2005, 1992). This work focuses on pits in a topographically smooth medium-toned deposit in a local basin distal to the Harmakhis Vallis system. The smooth deposit covers an area of ~10,000 km^2 and is bounded to the north, east, and south by raised ridges of possible tectonic origin (Tanaka & Leonard, 1995) and to the west and southeast by fractured chaos terrain (Glamoclija et al., 2011; Sharp, 1973). The area has been mapped as an early- or late-Hesperian basin unit noted for layering (Tanaka et al., 2014), as can be seen in the troughs west of the study area and at the base of the bounding ridge to the north. Centered on 41°S, 079°E, the pits of this study cluster to the east of troughs that crosscut the smooth terrain, and the pits decrease in number to the east, where eventually only a few crescent-shaped pits disrupt the smooth terrain. The field of pits covers an area of roughly 1,350 km^2 within the smooth deposit and includes $>$300 individual potential dune cast pits (Figure 1).

2.2. Pit Field in Noctis Labyrinthus

The second study area lies within Noctis Labyrinthus in a topographic low just northwest of Oudemans crater (Figure 2; Masson, 1977). This region of Noctis Labyrinthus has been mapped as a late-Hesperian transition unit characterized by smooth plains found between Noachian highland terrains (Scott & Tanaka, 1986; Tanaka et al., 2014). Beyond these highlands are Hesperian volcanic deposits, which have flowed into topographic lows. Centered on 07.8°S, 092.3°W, the series of pits at this study site interrupt a smooth deposit similar to pits in Hellas basin. This deposit extends across an area of ~10,000 km^2, onlapping topographic highs including crater walls and small mounds. Unlike the smooth deposit observed in Hellas basin, the pit-defining unit in Noctis Labyrinthus exhibits a regularly spaced erosional pattern in the southeast and meter-scale ridges of positive relief in the northwest. An exposed trough at the western margin of the deposit truncates the deposit, revealing a layered light toned material, possibly hydrated minerals (Mangold et al., 2010; Weitz et al., 2011), beneath the smooth plains-forming unit. The pits within the smooth deposit occur in a region around a 2-km-diameter crater and cover an area of ~250 km^2. The area includes $>$480 potential dune casts, and modern eolian material forms abundant small bedforms across the region.

3. Methods

The lengths, widths, and orientations of putative dune casts were measured at each study site using images from the Mars Orbiter Context Camera (CTX; ~5 m/px; Malin et al., 2007) and High Resolution Imaging Science Experiment (HiRISE; 25 cm/px; McEwen et al., 2007). In modern dunes, length is measured from the point of maximum curvature on the lee face to the furthest position on the stoss in the direction normal to the dune crest trend (Figure 3e). Lee faces of modern barchan dunes form normal to the transport direction in unidirectional winds (Hersen, 2004; Parteli et al., 2014) or normal to the resultant direction of multiple wind vectors in a more complex wind regime (Rubin & Hunter, 1987). When sand supply is limited, dunes can also form by asymmetric elongation, developing in the *fingering mode* of Courrech du Pont et al. (2014). Most pits exhibited some relict curvature on the interpreted lee face and general north-south elongation in the interpreted transport direction. The lengths of pits were measured using the modern dune convention, and the azimuth of the length measurement was used to represent orientation and

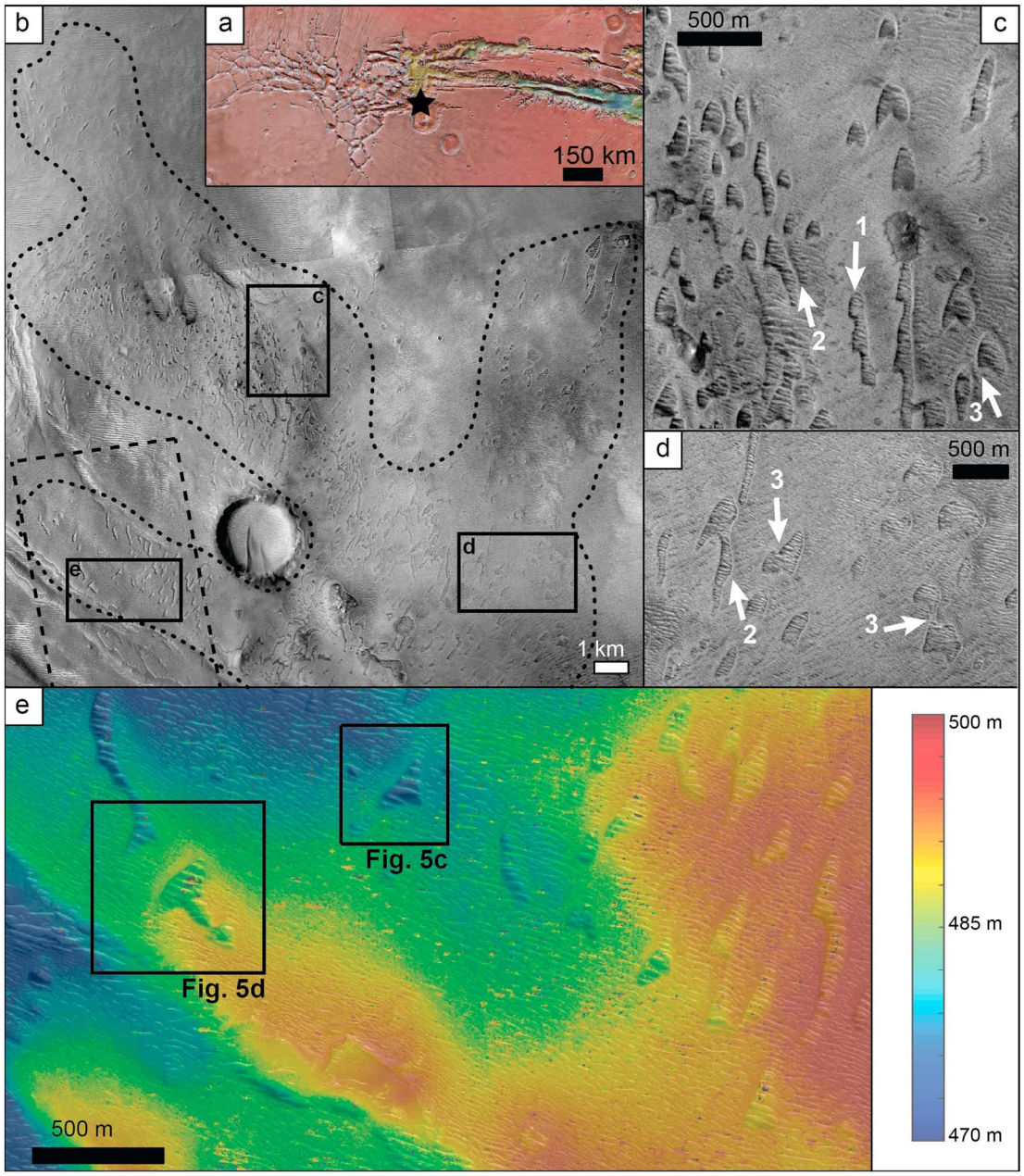

Figure 2. Dune cast pits in Noctis Labyrinthus. (a) Location of study area (black star). The field sits just northwest of Oudemans crater. (b) The extent of pits preserving the putative dune field and the locations of other panels are shown by dotted line and boxes, respectively. A High Resolution Imaging Science Experiment (HiRISE) digital elevation model was created from the only available HiRISE coverage in this region, the extent of which is shown in the lower left (dashed line). (c) Pits exhibiting characteristic barchan morphologies. Note the chains of calving dunes (1), elongating arms (2), and interacting pits (3). Most pits are approximately symmetrical and of a scale similar to modern dunes on Mars. Note the linear features concentrated in the dune pit interiors that are interpreted as modern eolian bedforms. (d) Pits exhibiting dune interaction morphologies (3) and elongating arms (2). (e) Colorized elevation over HiRISE image across pits in the southwest margin of the field. Pits are barchanoid and elongated in this region. The digital elevation model also picks up transverse eolian ridges occupying the bottom of the pits. HiRISE images ESP_048967_1720 and ESP_047965_1720. North is up in all figures.

the inferred transport direction. Width on modern dunes is measured from horn to horn (the pointed terminations extending downwind on a barchan; Figure 3e). For the Martian pits, width was measured as the longest distance normal to the measurement of length.

The depth of the pits could only be measured in the Noctis Labyrinthus field, because no HiRISE image coverage or stereo CTX coverage of the Hellas basin pits was available at the time of this study. At the Noctis

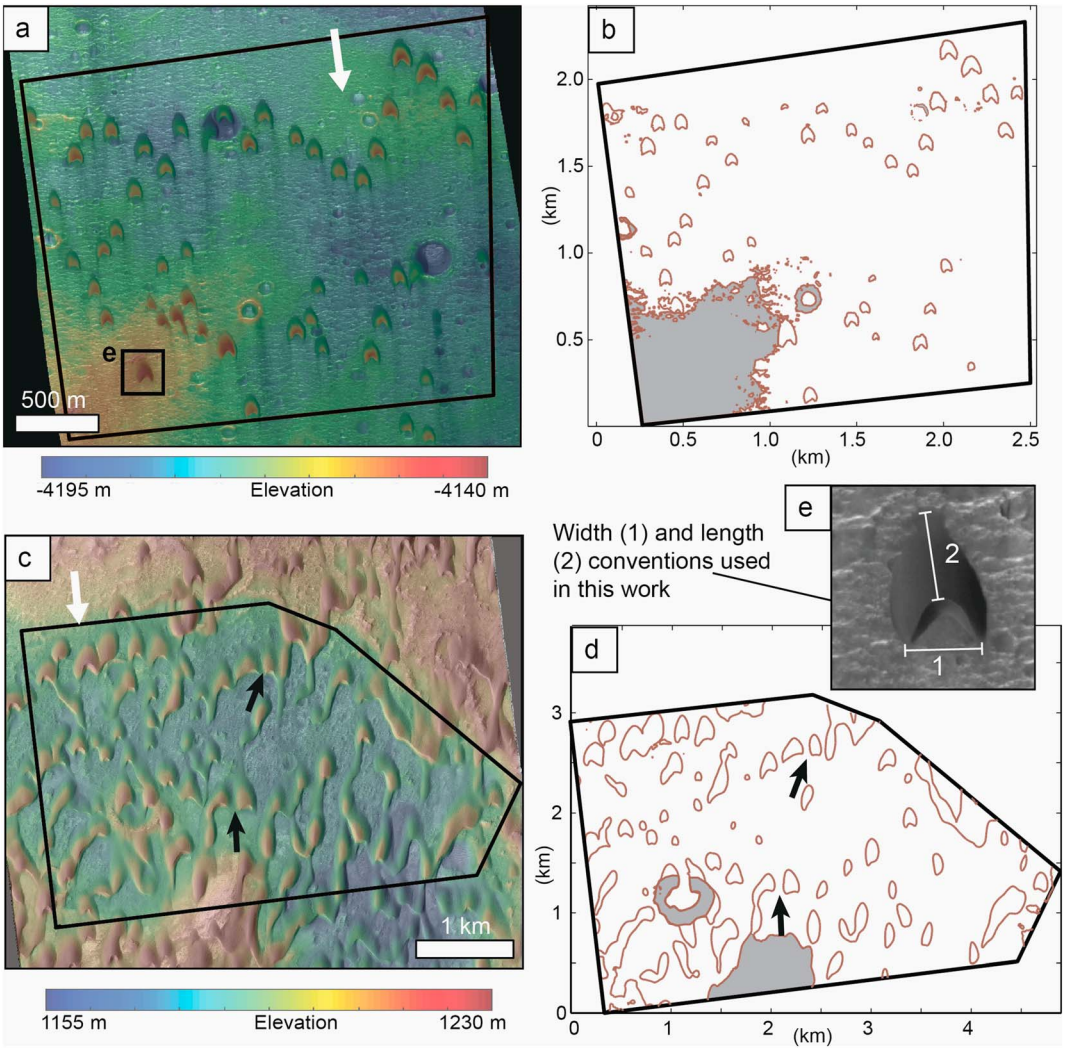

Figure 3. Modern Martian dunes and modeled pit morphologies. (a) Isolated barchan dunes in Oyama crater. High Resolution Imaging Science Experiment image stereo pair: ESP_042424_2035/ESP_042714_2035. (b) Model pit morphologies generated by artificially flooding topography in (a) to an equipotential surface averaging 6 m in depth (the mean depth of measured Noctis Labyrinthus pits). Lines indicate where topography in (a) intersected the horizontal surface. Dunes are interpreted as erodible material, which would be removed, leaving pits with the outlines shown. Gray shaded regions in (b) and (d) indicate nondune topography above the equipotential surface. (c) Barchan and barchanoid dunes in Herschel crater. Note the abundant interactions (collisions) between dunes and the many asymmetrically elongating arms. Small black arrows show interactions that are not preserved in the modeled pit morphologies in (d). High Resolution Imaging Science Experiment image stereo pair: PSP_002860_1650/PSP_003572_1650. (d) Model pit morphologies constructed as in (b) but using topography from (c). Note the interactions seen in (c) are not all preserved in (d). (e) Example barchan dune with the width and length measuring conventions used in this work. Note the dune terminations that form points of the barchan crescent. Large black arrow indicates the inferred migration direction. Digital elevation models courtesy of National Aeronautics and Space Administration/Jet Propulsion Laboratory.

Labyrinthus study site, overlapping HiRISE images (EPS_048967_1720 and ESP_047965_1720) were used to construct a digital elevation model (DEM) using the Integrated Software for Imagers and Spectrometers developed by the U.S. Geological Survey in tandem with the Ames Stereo Pipeline (Figure 2e; Shean et al., 2016; Sides et al., 2017). The resulting DEM has a spatial resolution of 1 m/px, and elevation profiles were generated by linear interpolation between these points. Pit depths were taken as the difference in elevation from the lowest and highest points along the profile.

Two modern dune fields on Mars with existing HiRISE DEMs were also measured to compare the geometries of modern Martian dunes and the putative dune-formed pits. The length, width, orientation, and height of

Table 1
Measured Geometric Parameters for Pits and Modern Dunes With Uncertainty of ±1σ

Measurement	Noctis Labyrinthus	Hellas basin	Herschel crater (modern)	Oyama crater (modern)
Length				
Mean (m)	177 ± 67	327 ± 113	231 ± 72	176 ± 31
Number of measurements	475	316	110	59
Width				
Mean (m)	136 ± 52	402 ± 125	211 ± 63	157 ± 29
Number of measurements	475	316	110	59
Height				
Mean (m)	5.9 ± 1.2	—	18.5 ± 6.0	13.5 ± 4.0
Number of measurements	31	—	108	59

isolated barchan dunes in Oyama crater and crescentic and barchanoid dunes in Herschel crater were measured as per the methods above. The two sites host dunes of sizes and morphologies common to modern eolian dunes on Mars (e.g., Day & Kocurek, 2016; Fenton & Hayward, 2010; Hayward et al., 2014), and the modern dunes are similar in scale to the size of the pits studied in Noctis Labyrinthus and Hellas basin. All measurements of modern dunes were made using HiRISE images and existing DEMs in the National Aeronautics and Space Administration Planetary Data System.

Dunes in Oyama and Herschel craters were also used to model what morphologies would form from partial burial and erosion of a dune field. Modeled pits were generated by extracting intersections between the DEM of dune topography and a horizontal plane representing an equipotential surface of interdune-filling material. The height of the surface was set such that the average depth to the underlying topography equaled the average pit depth measured in the Noctis Labyrinthus. The intersections between plane and dune topography are shown in Figure 3 and represent the modeled outlines of pits formed from partial dune burial. These synthetic pits were measured for length, width, and orientation, as per the actual Martian pits in Noctis Labyrinthus and Hellas basin.

To constrain the lithology of the smooth deposits that surround and define the pits, the thermal inertia of both study areas was mapped using overlapping daytime and nighttime Thermal Emission Imaging System (THEMIS) images. Following the methods of Catling et al. (2006), radiance values over the study areas were used in conjunction with Mars Orbiter Laser Altimeter topographic data to estimate the apparent thermal inertia. The procedure requires aerosol optical depths of <0.30 as measured for ice and dust clouds in THEMIS Bands 9 and 5, respectively. This condition was met for both study locations using daytime image I08142023 and nighttime image I08024017 in Noctis Labyrinthus and daytime image I07313002 and nighttime image I18077017 in Hellas basin.

4. Results

4.1. Pit Scale, Variability, and Comparison to Synthetic Dune Casts

As summarized in Table 1, the length, width, orientation, and vertical relief of pits in the two study areas and modern dunes in the two modern analog locations were measured to assess whether pit morphologies could reflect an eolian dune origin. All uncertainties are given as plus or minus one standard deviation. In the Hellas basin, 316 pits were measured with a mean width of 402 ± 125 m and a mean length of 327 ± 113 m. Depths could not be measured at this locale, because of the lack of high-resolution stereo image coverage, as noted in section 3. Assuming the pits reflect dune morphologies, the inferred migration direction averaged 186° ± 11° (Figure 4b). In Noctis Labyrinthus, the 475 measured pits had mean widths of 136 ± 52 m, mean lengths of 177 ± 67 m, and a mean southward migration direction of 191° ± 10° (Figure 4a). Of the studied pits, 31 pits fell within the HiRISE DEM coverage and were found to have a mean depth of 5.9 ± 1.2 m (Figure 5). Modern eolian features, including transverse eolian ridges and ripple fields, occupied many of the pits in Noctis Labyrinthus, sometimes covering a substantial percentage of the bottom of the pits (Figure 5). The presence of these loose sands suggests that the measured depths represent a lower bound on the actual pit depths. However, given the scale of the features

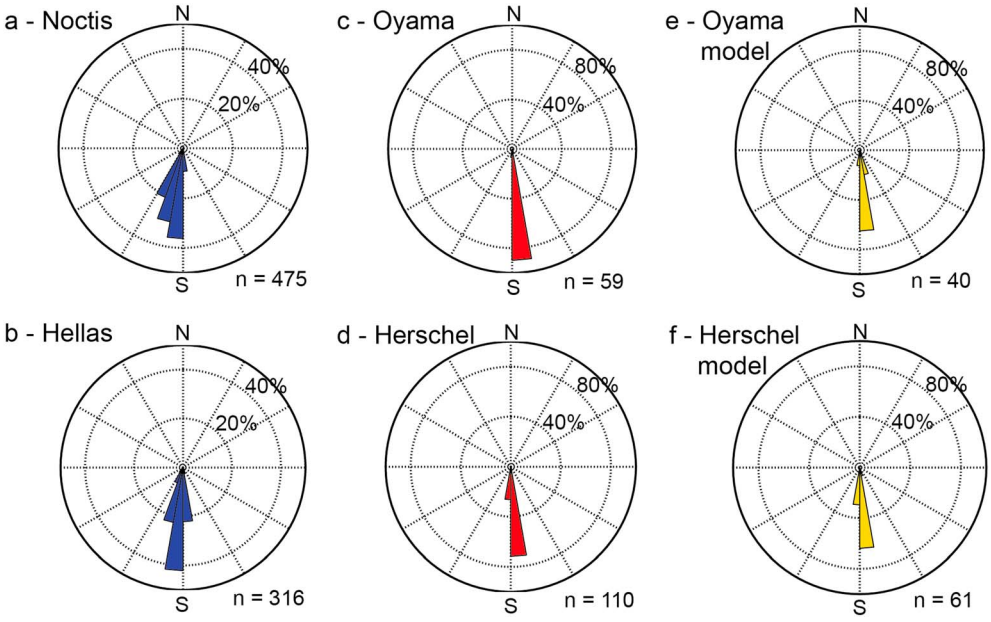

Figure 4. Inferred migration directions measured from pit and modern dune morphologies. (a and b) Migration directions interpreted from the studied Martian pits are shown in blue. (c and d) Modern dunes are shown in red. (e and f) Measurements of the synthetic pits generated from modern dune topographies are shown in yellow. The specific locations are noted before the letter in the upper left of each subpanel. The number of measurements for each is noted in the lower right.

seen in the pits and the incomplete coverage of the pit floors, it is unlikely that any pits are much deeper than the maximum measured depth of 8 m.

Dunes in Oyama and Herschel crater were measured for comparison with the Martian pits. In Oyama crater, the 59 barchan dunes were measured and inferred to have an average migration direction of 174° ± 3° (Figure 4c). These dunes had an average width of 157 ± 29 m and average length of 176 ± 31 m. The height of the dunes was measured along the length of the dune, taking the elevation difference between the crest and base of the lee face. The Oyama crater dunes had a mean height of 13.4 ± 4.0 m, approximately twice as high as the Noctis Labyrinthus pits are deep. Using topographic data from the Oyama crater study area, synthetic pit outlines were modeled by filling the interdune areas to an equipotential surface with an average depth of 6 m (see section 3). The points of intersection between this surface and the dune topography represent the outlines of pits that would form if the loose dune sands were to erode away and the interdune deposit remain (Figure 3b). A subset of the total study area was used to generate synthetic pits. After artificial flooding (or burial) (Figure 3), 40 of the 50 included dunes protruded above the equipotential surface (i.e., 80% were modeled to leave a dune cast pit). The synthetic Oyama pits measured an average of 115 ± 34 m in length and 139 ± 40 m in width or roughly ~65% and ~89% of the original dimensions, respectively. The measured orientation changed only slightly, becoming 173° ± 5° (Figure 4e).

The same exercise was performed with the modern dunes in Herschel crater (Figure 3c). Dominantly barchan and barchanoid dunes, the 110 dunes in this study area were found to have a mean width of 211 ± 63 m and mean length of 231 ± 72 m. These dunes are also interpreted to be migrating toward the south with a mean migration direction of 178° ± 3° (Figure 4d). Standing at an average height of 18.5 ± 4.0, a subset of the dunes in Herschel crater were again used to model synthetic dune casts by flooding (or burying) the field with an arbitrary material to an equipotential surface with a mean depth of 6 m. The resulting 61 pits (constituting 95% of the 64 synthetically flooded dunes) had a mean width of 146 ± 62 m and length of 175 ± 70 m, roughly 69% and 76% of the uncovered values, respectively. As with the Oyama synthetic example, the orientation remained similar to the modern measurement, averaging 177° ± 4° (Figure 4f). In summary, synthetic pits made from barchan dune topography and 6 m of interdune burial (1) preserve the original dune migration direction with only slightly higher variance than when measured from the original dunes, (2) capture

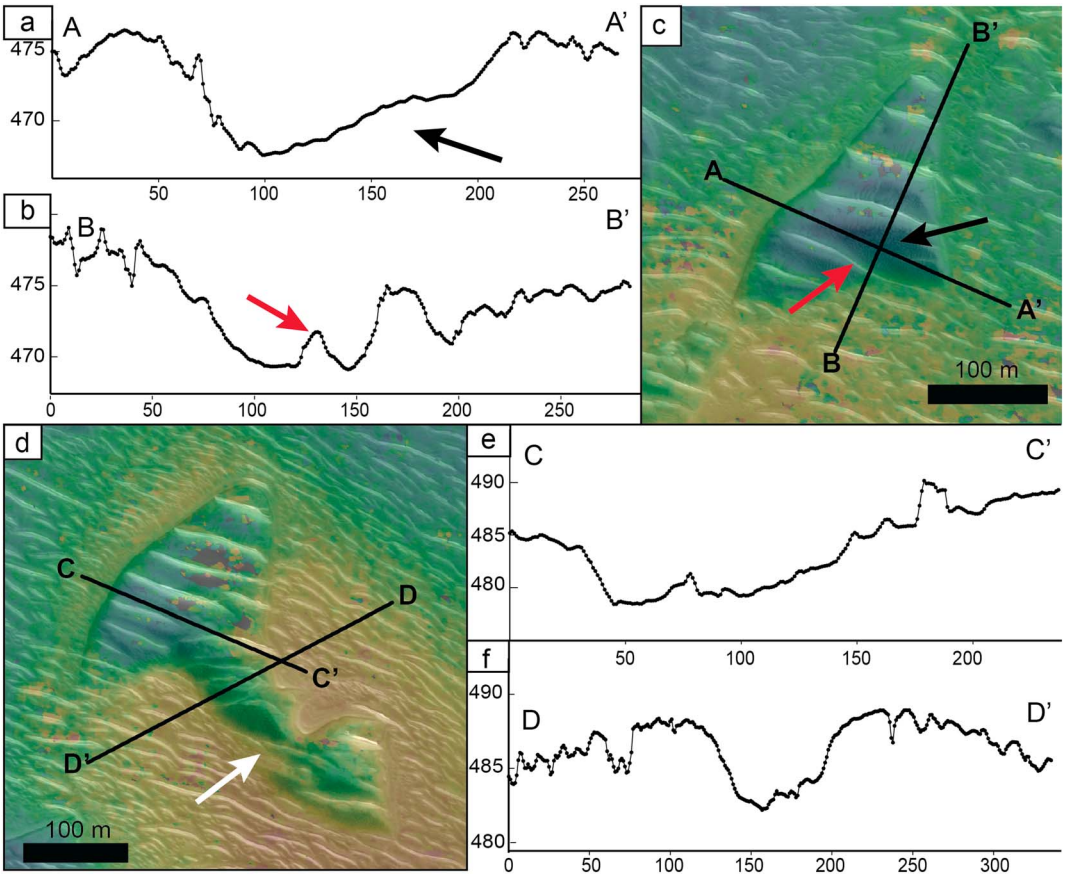

Figure 5. Topographic profiles across dune cast pits in Noctis Labyrinthus. (a) Topographic profile of transect A–A′ in (c). The rise in elevation within the pit is attributed to a dark sand ripple field that can be seen in (c) (black arrows). (b) Topographic profile of transect B–B′ in (c). This transect is in the interpreted transport direction of the dune and crosses transverse eolian ridges occupying the dune pit (red arrows). (c) High Resolution Imaging Science Experiment digital elevation model of an individual dune pit with transects for profiles in (a) and (b). Arrows correspond to features highlighted in (a) and (b). (d) High Resolution Imaging Science Experiment digital elevation model of a dune interaction (white arrow) between larger barchan (upper left) and small barchan (lower right). Transects correspond to profiles in (e) and (f). (e) Topographic profile of transect C–C′. (f) Topographic profile of D–D′. All units are in meters.

between 80% and 95% of the original dunes, and (3) exhibit mean length and width values ~70% of the original dune measurements.

4.2. Smooth Deposits Surrounding the Pits

Pits in both Noctis Labyrinthus and Hellas basin are surrounded by smooth deposits that extend beyond the limits of the pit field. In both locations, the smooth deposits are bounded by local topographic highs and the areal extent of each deposit was measured to where it met these barriers. Deposition of related material outside the local basin in which the pits are found is outside the scope of this work. Within the studied local basins, each deposit covers an area of ~10,000 km^2, and assuming an average depth of 6 m as measured in Noctis Labyrinthus, each deposit has a similar volume of ~60 km^3.

The thermal inertia of the smooth deposits was estimated using THEMIS day and night infrared imaging (Figure 6 and see section 3). At each location, the thermal inertia of areas of the smooth deposit away from pits and other obstructions was recorded (white arrows in Figure 6), as well as the thermal inertia inside pits (black arrows in Figure 6a). In Hellas basin, the smooth deposit as a whole decreases in thermal inertia from west to east, with a maximum of 450 $J \cdot m^{-2} \cdot K^{-1} \cdot s^{-1/2}$ in the west, decreasing to 340 $J \cdot m^{-2} \cdot K^{-1} \cdot s^{-1/2}$ in the east with isolated pixels capturing a minimum in the area of 300 $J \cdot m^{-2} \cdot K^{-1} \cdot s^{-1/2}$ The pits in Hellas basin are large with respect to the 100-m/px THEMIS map resolution, and the pit interiors clearly

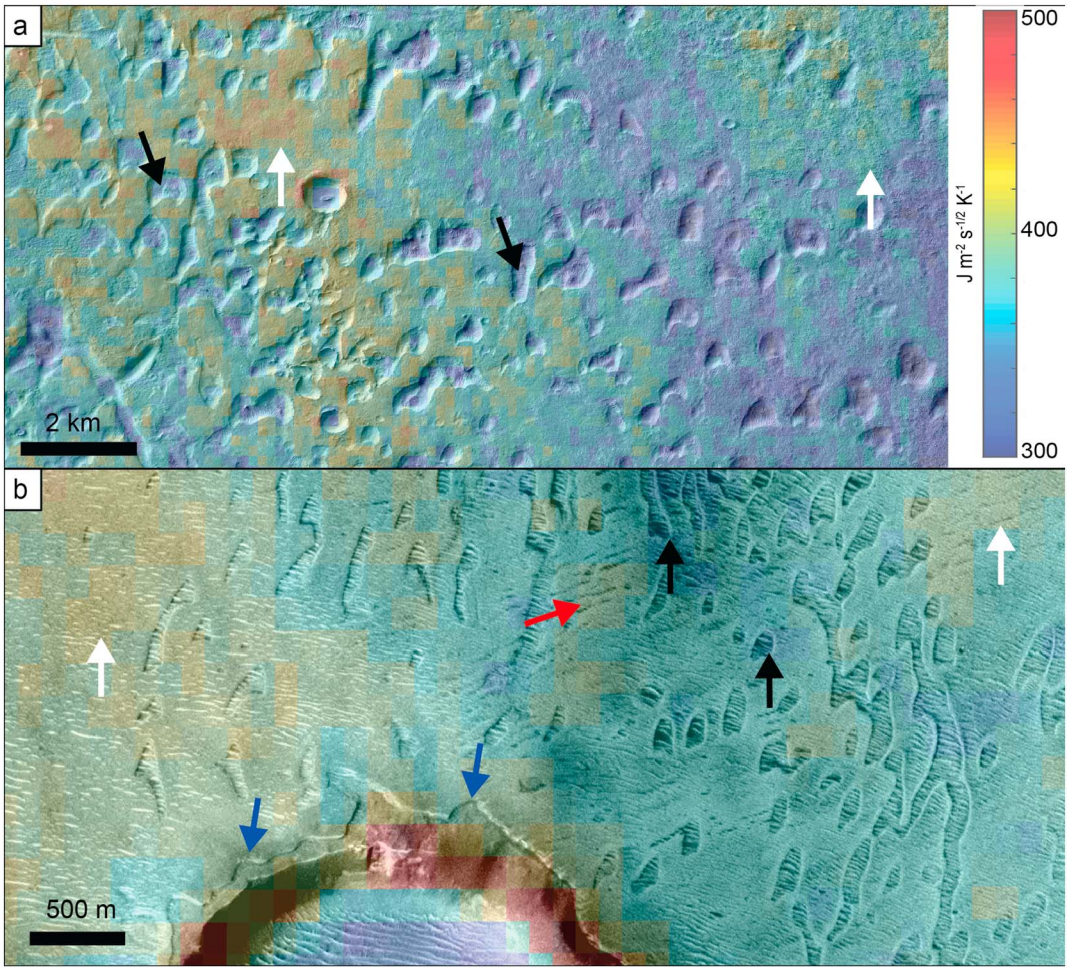

Figure 6. Colorized Thermal Emission Imaging System thermal inertia overlain on CTX images of pit fields. (a) Pits in Hellas basin. The smooth deposit between pits shows a general decrease in thermal inertia from west to east; however, across the study area the thermal inertia of the smooth deposit (white arrows) is relatively high compared to the measured thermal inertia in the pits (black arrows). This difference may be a function of loose eolian material trapped in the pit interiors. (b) Pits in Noctis Labyrinthus. The thermal map pixel size (~100 m) in this image is much larger with respect to the size of the pits. Nevertheless, as in (a) the areas sampling the smooth deposit exhibit relatively high thermal inertia (white arrows), and the areas sampling part of the pit interiors exhibit relatively low thermal inertias (black arrows). This image also shows the smooth deposit apparently onlapping onto the uplifted crater rim (blue arrows), and lineations trending ENE-WSW that could be compression ridges from lava-flow deposition (red arrow). Thermal inertia was derived from daytime and nighttime Thermal Emission Imaging System images (see section 3). CTX images are the same as in Figures 1 and 2.

correlate with mapped areas of low thermal inertia. This presumably indicates the presence of loose eolian material concentrated in the pits, as is also seen in images in Noctis Labyrinthus. The decreasing thermal inertia eastward across the smooth deposit could also be attributed to eolian cover. Eolian deposits even only a few centimeters thick can mask the thermal signature of underlying more competent material and may not be resolvable in CTX images.

Similar results were found in Noctis Labyrinthus where the maximal thermal inertia recorded on the smooth deposit was 420 $J \cdot m^{-2} \cdot K^{-1} \cdot s^{-1/2}$ (white arrow in Figure 6b). Pits at this study site are notably smaller than those in Hellas (< 2 THEMIS pixels wide), and the strong correlation between pit location and low thermal inertia observed in Hellas was not as evident at the Noctis Labyrinthus site. Locations of lower thermal inertia (<350 $J \cdot m^{-2} \cdot K^{-1} \cdot s^{-1/2}$) were found more frequently in regions of dense pits. The lowest thermal inertia measured in the study site was in the interior of the 2-km-diameter crater south of the pit field. This crater is filled with modern eolian bedforms densely covering an area many hundreds of square meters, and the

thermal inertia recorded over this eolian material was 340 $J \cdot m^{-2} \cdot K^{-1} \cdot s^{-1/2}$. Given the abundance of modern eolian bedforms seen in images both on the surface of the smooth deposit and concentrated in the pit interiors, we interpret that most of the THEMIS pixels are capturing at least some component of modern eolian material in this area. For both study sites, assuming the smooth deposit represents a homogenous unit beneath some uneven eolian cover, the highest measured thermal inertia values would represent a lower bound on the thermal inertia of the unit. The measured values are too low to suggest the smooth deposit represents exposed Martian bedrock (Edwards et al., 2009), but the values are consistent with elsewhere interpreted sedimentary rocks (Catling et al., 2006; Christensen et al., 2003) or partial obscuration of bedrock by eolian cover (Fergason et al., 2006).

5. Discussion

5.1. The Case for an Eolian Origin

Several separate lines of evidence suggest that the pits in Noctis Labyrinthus and Hellas basin formed originally from eolian barchan dunes. The distribution of the pits, their particular morphologies, and the geologic context all point to an eolian origin. In general, Martian dunes cover a range of spatial scales similar to dunes on Earth. Dune heights range from ~ 4 m on the lower end (Ewing et al., 2017), to a maximum measured dune height of >450 m (Lorenz et al., 2015), with typical values in the few tens of meters range (Bourke et al., 2006). Lengths and widths vary widely depending on dune morphology. In all of the measured parameters, the pits in this study are of a scale consistent with observed dunes on modern Mars (Day & Kocurek, 2016; Fenton & Hayward, 2010; Hayward et al., 2014).

The orientations of the studied pits also cover a limited range, consistent with an origin in eolian dunes (Figure 4). Orientations from the pits span a slightly wider range of orientations than the modern analogs, but this increased variance was also observed in the modeled pits relative to their modern counterparts. Several reasons could account for the variation: (1) the studied pit fields cover a large areal extent allowing for more interaction between wind and local topography that might cause variations in wind regime within the field, (2) the pits preferentially preserve the largest dunes which take longer than small dunes to reorient to changes in wind regime and may reflect older winds or winds integrated over long enough time to capture some variability, and (3) orientations inferred from pits are necessarily more uncertain than those inferred from active dunes because the pits express only a degraded outline of the dune morphology, rather than complete lee and stoss slopes. Regardless, both modern dunes and pits have a tight range of orientations typical of eolian dunes on Mars.

The morphologies of the pits observed in this study provide the most compelling evidence for their origin as eolian dunes. In general, the pits exhibit crescentic shapes characteristic of barchan and barchanoid dunes. The existence of any single crescent-shaped pit would not be sufficient to justify the interpretation of formation from a dune field. However, the number, spacing, and orientation of the observed pits are consistent with a partially buried dune field. Furthermore, although the majority of the pits have a muted crescentic morphology compared to modern barchans, some pits express morphologies so similar to modern dunes that they are easily mistaken for actual dunes if the viewer is not paying attention to the direction of the sun (e.g., Figure 1d). Although some might argue that the absence of barchan crescent points (also called horns or terminations) in some pit morphologies discredits the interpretation of an eolian origin, here we argue the reverse. Dune terminations are topographically lower than the dune crest and would be among the first parts of a dune covered during partial burial. Those pits where crescent points are absent reflect only the uppermost portion of the paleodune. Synthetic dune pit morphologies generated from Herschel crater demonstrate how oblong and blunted triangle-shaped pits can result from modern barchanoid dunes.

In both study areas, individual pits and groups of pits exhibit morphologies characteristic of eolian dune migration. Among the larger pits, several instances exhibit an asymmetric shape, with one crescent arm elongating in the interpreted downwind direction (Figures 2c and 2d). This morphology is common among dunes on Mars, in particular (Bourke, 2010; Parteli et al., 2014), where barchan dunes migrate in a sediment limited fingering mode often associated with bimodal winds and limited sand supply (Courrech du Pont et al., 2014). Among the smaller pits, some form chains of oblong to crescent-shaped pits offset laterally in one direction (Figure 2d). This morphology is recognized in modern dunes as resulting from calving of smaller dunes from a

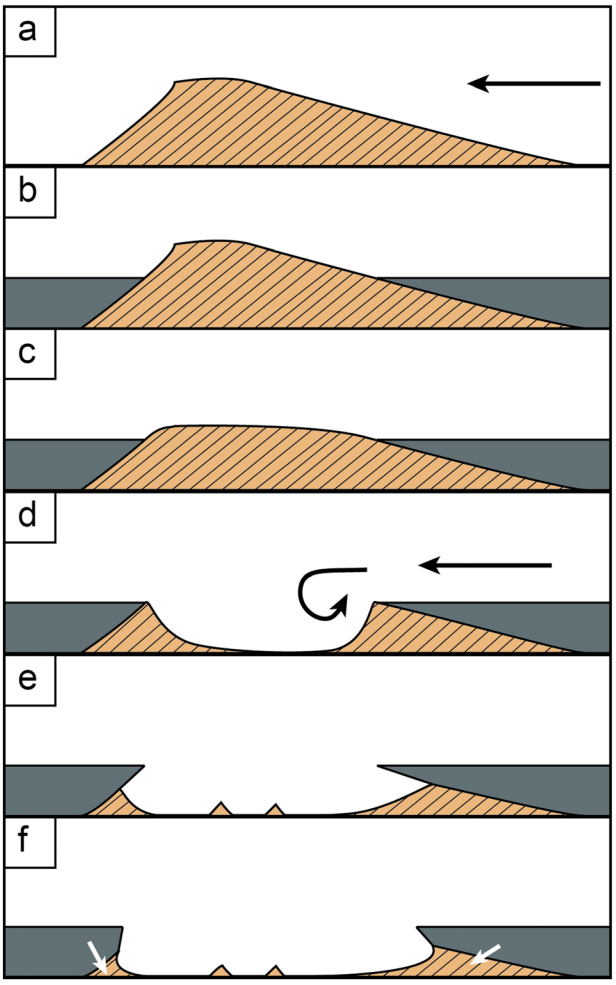

Figure 7. Cartoon of proposed dune pit formation. (a) Barchan dunes are active at the Martian surface. Black arrow indicates wind direction; thin black lines represent dune strata from migrating lee face. (b) Interdune areas are flooded to roughly half the dune height by an unknown material, possibly basalt or subaqueously deposited sediments. (c) Uncemented dune sands erode away. (d) When dune sands erode below the depth of the interdune deposit, a separation cell of recirculating flow (curled arrow) forms allowing for further scour. (e) Pits from eroded dune material are topographic lows in which modern eolian sediments are trapped, forming small bedforms. An overhang potentially forms in cemented interdune material. (f) The potentially undercut margin of the interdune deposit erodes, widening the pit. White arrows indicate where ancient strata are predicted to be preserved and shielded by overlying interdune deposit.

larger parent body, or as the reworking of an existing dune in limited sediment conditions (Gao et al., 2015; Kocurek et al., 2010; Worman et al., 2013).

Additionally, the outlines of apparent dune interactions are found in Noctis Labyrinthus pits (Figures 2c and 2d). Dune interactions are abundant in modern dune fields and occur in a variety of well-studied morphologies (Brothers et al., 2016; Ewing & Kocurek, 2010; Kocurek et al., 2010). The number of interpreted interactions in the pit fields is low compared to modern fields. Dune interactions occur at dune terminations, however (Ewing et al., 2006; Werner & Kocurek, 1999), and would be among the first attributes covered by flood material, thus obscuring recent or incipient interactions between large dunes. This is evident in the synthetic pits made from dunes in Herschel crater (Figure 3c) where interactions are abundantly occurring between the modern dunes but are not all preserved in the morphologies of the pits (Figure 3d).

The pit morphologies observed in Noctis Labyrinthus and Hellas basin so closely match the plan view shapes of modern dunes and capture the diverse behaviors of modern bedforms, that the number and diversity of these examples suggest an origin in eolian dunes rather than coincidental resemblance. The preponderance of evidence suggests that the studied pits formed from the partial burial of a dune field, from which dune sands were later removed, leaving the observed ghost dune pits as a field of muted-barchan-shaped hollows (Figure 7).

5.2. What Flooded the Dune Field?

The morphologies of the observed pits point strongly to an origin in eolian dunes, partially buried by an interdune flood of material. However, this begs the question: what flooded the dune field? The apparent minimal disruption of the dune morphologies requires a low-energy emplacement mechanism. Terrestrial instances of flooded and preserved dunes have been dominantly caused by basalt flows (Gaylord et al., 2016; Jerram et al., 2000; Waichel et al., 2008), making basalt a natural candidate for the smooth deposits on Mars. Flooding by water has also occurred on Earth, preserving the dunes in at least one case with postflooding marine limestone deposition (Benan & Kocurek, 2000). Examples of modern dunes partially submerged in lacustrine settings can be observed in Moses Lake, Washington (Bandfield et al., 2002; Petrone, 1970), and Lake Chad (Durand, 1982).

In Noctis Labyrinthus, the geologic setting of the study area, in a topographic low downslope of known volcanic deposits, makes a basalt flow interpretation of the smooth deposit particularly plausible. The extensive tectonic activity and volcanism associated with the formation of the region (Carr, 1974) could account for the origin of the potential basalt flows. Unfractured basalt has a thermal inertia of $>$2,000 $J \cdot m^{-2} \cdot K^{-1} \cdot s^{-1/2}$ (Robertson, 1988), but the much lower value measured on the smooth deposit at the Noctis Labyrinthus study site could be attributed to eolian cover and integration of the large pixel footprint. The higher thermal inertia of the smooth deposit as opposed to the regions where eolian bedforms are concentrated suggests that at the very least the underlying material is some competent rock. This is supported by the craters observed on the smooth deposit and the presence of the sharp-sided pits themselves. The linear features on the smooth interdune deposit (Figure 6b) could be interpreted as small wrinkle ridges in a basalt flow formed from compression at the top of the flow. These lineations form nearly orthogonal to the modern eolian bedforms and are thus easy to distinguish even when the two are superimposed.

An alternative origin for the smooth deposit is suggested by a previous interpretation of fluvial activity in Noctis Labyrinthus. Rodriguez et al. (2016) attribute the low-lying deposits in this region to deposition by water when an elevated aquifer in the Tharsis region drained into topographic lows in Noctis and later Valles Marineris. Such drainage could occur slowly, fulfilling the requirement that interdune deposition be low energy, and only partial burial could be accounted for by the many different paths such drainage could take. Even in the case where the dune field were completely submerged beneath water, deposition in the interdune might still take place. Pelagic sedimentation of fines settling out of the water column would be expected to drape the dunes, similar to the carbonate-draped dunes in the abovementioned example on Earth (Benan & Kocurek, 2000). Sediments draped on the dunes might be thicker in interdune areas from gravitational slumping, but overall, the deposit thickness would be of similar order and the observed pits would not form without substantial erosion of both the interdune and draping deposit. Alternatively, subaqueous deposition could occur preferentially in the submerged interdune areas if hyperpycnal flows from the local basin walls carried sediment to the area (Lamb & Mohrig, 2009; Mulder et al., 2003). These high-density, sediment-laden, turbidity currents hug the base of the water column and could be deflected around dunes which would act as local obstacles to flow.

In Hellas basin, nearby fluvial and volcanic features suggest similar mechanisms might have affected both Hellas and Noctis Labyrinthus. The studied pit field in Hellas basin lies in a topographic low distal to the fluvially cut channel system of Harmakhis Vallis (Price, 1998) and distal to volcanic channels originating at Hadriaca Patera (Crown & Greeley, 1993; Williams et al., 2007). Although the mapped extent of volcanic deposits related to Hadriaca Patera does not extend to our study area (Crown & Greeley, 2007), the proximity of a source of lava flows and the downslope location of the pit field suggest a basalt flow origin merits consideration. As seen in Noctis Labyrinthus, the smooth deposit in Hellas basin has a higher thermal inertia compared to the sand-trapping pits. However, in Hellas the measured thermal inertia across the smooth deposit is variable and decreases to the east. Again, this could represent eolian cover not resolvable in the CTX image, or this could suggest an alternative origin for the deposit. Troughs to the west of the study area cross cut the smooth deposit, and the ridging seen in Noctis Labyrinthus is not present here.

The position relative to Harmakhis Vallis suggests that deposition may account for the smooth deposit. High-energy fluvial activity more proximal to and associated with the Harmakhis system would likely erode the dune morphologies and transport the loose sands away. However, positioned at the distal end of the Vallis, it is possible that low-energy fluvial events carried fines into the local topographic basin, flooding the paleointerdune areas and depositing fine grained sediment from suspension (Ahlbrandt & Fryberger, 1981; Loope & Rowe, 2003). Such deposition could have been continuous or intermittent. As with the Noctis field, the depth to which the dunes were submerged in such a case remains unknown. Identification of the smooth deposit as a turbidite would suggest deep water at the time of deposition, and identification of evaporites would suggest shallow water. Differentiating such interpretations would require future surface-scale observations or high-resolution spectral imaging.

Additional mechanisms for depositing large amounts of interdune material on Mars include ash fall and eolian sedimentation. Ash deposits could have buried dune material, but in such a case the deposits would be expected to drape the dunes rather than concentrate in the interdune region. After the 1980 eruption of Mount St. Helens, dunes in the Moses Lake region of central Washington were covered by a several-centimeter-thick layer of ash that continued to drape inactive bedforms for the subsequent decade (Edgett & Lancaster, 1993). We assume that the 6 m of deposition in the interdune area would halt the activity of the dunes, in which case the Moses Lake example suggests ash fall would preserve the dunes in positive relief rather than negative. Additionally, the smooth deposits exhibit no signs of erosion and significant erosion would be necessary to remove a ~6-m draping ashfall deposit.

An eolian interpretation of the interdune material is rejected, because unrealistic mechanisms must be invoked to preserve the interdune but not the dune material. Eolian fill of the interdune is possible if a dune field becomes indurated or sediment supply rapidly increases. However, if the dunes were indurated, they would not be removed preferentially over the interdune material. If they were not indurated, then it is unlikely that the interdune and dune material would differentially cement and homogenous erosion would be expected. A mechanism to temporarily indurate the active dunes and then permanently indurate the interdune deposit, without interacting with the dune material, is unlikely, leaving basalt flows and subaqueous deposition the most likely candidates for the flood deposit origin.

5.3. Other Pit Formation Mechanisms

Other types of pits and pitted terrains are common on Mars and have variously interpreted origins ranging from impact cratering (Wyrick et al., 2004), to sublimation (Carr, 2001), to karstic dissolution (Spencer & Fanale, 1990). For the most part, these origins can be easily ruled out for the pits in this study by the scale or morphology of features associated with these alternative interpretations (e.g., impact craters are circular whereas the studied pits are not). Although sublimation could form pits of the scale in this study and with variable morphologies (Kadish et al., 2008), both locations in this study are equatorial of 45° and ice-related processes are unlikely to dominate the surface geomorphology.

The studied pits bear morphological similarity to flute scours on Earth. Flute scours form from the interaction of turbulent fluvial systems and an erodible bed (Allen, 1968) and have been identified at scales similar to the studied Martian pits in marine settings on Earth (Normark et al., 2009). Flute scours also exhibit the crescentic shape typical of modern barchan dunes, but flutes are distinctly negative topographic features, as are the pits in this study. The morphological similarities between the two are intriguing; however, flute scours are deepest at the apex and shallow toward the terminations, which was not observed in the studied Martian pits. Furthermore, no other evidence of erosion was found to suggest that the smooth deposits on Mars have been highly scoured.

Large-scale fluvial processes, including catastrophic flooding, can cause the formation of pits from scour and abrasion by turbulent vortices (kolks). Although catastrophic flooding has been hypothesized to have occurred on Mars (Baker & Milton, 1974), the locations studied in this work are not near the topographic boundaries where such flooding may have been. In addition, a kolk-scour origin would imply that the measured migration directions correspond with hydrodynamic alignment in the water flow direction, which in the case of Noctis Labyrinthus would be normal to the expected west-to-east flow direction. Finally, although some variability exists in pit morphologies, pits formed from high-energy fluvial scour tend to be circular or oblate, rather than crescentic, as evidenced by terrestrial potholes formed during megafloods in the Pleistocene (Baker, 2009).

5.4. Implications of Preserved Ancient Dune Fields

Assuming the two studied pit fields formed from partially buried ancient dunes, information about the ancient environment can be inferred from the pit morphologies. The ancient dune morphologies indicate that ancient northerly winds dominated transport in both study sites at the time of interdune deposition (see section 4.1). Symmetric barchan dunes are morphologically indicative of a single dominant wind direction (Hersen, 2004). The majority of the interpreted paleodunes appear symmetrical, but some asymmetrically elongating arms of paleodunes are seen in Noctis Labyrinthus (Figures 2c and 2d). These suggest a subordinate component of westerly or northwesterly wind is present, but transport is still dominantly from the north (Bourke, 2010; Parteli et al., 2014). If multiple wind directions of similar magnitude did exist, such a case would be reflected in the dune morphologies which would form transverse or longitudinal dunes in accordance with the divergence angle between the winds (Gao et al., 2015; Rubin & Hunter, 1987), rather than forming barchan dunes as observed.

We can compare these inferred ancient winds with modern wind vectors from the Mars Climate Database (Forget et al., 1999; Millour et al., 2015). Modern winds across Noctis Labyrinthus originate from the northeast for all seasons except northern summer (L_s 90°) when the winds originate from the east. In Hellas basin, winds come from the east in southern summer and fall and from the southeast and northeast in winter and spring, respectively.

Several explanations could account for the differences between inferred ancient and modeled modern wind regimes, including the following: (1) the modern wind regime is very different from the ancient when sand-transporting winds came dominantly from the north, (2) only winter winds were of sufficient strength to move sand, and the direction of the winds has changed only slightly over time, (3) the scales of circulation patterns and grid spacing in the global circulation model are large compared to the local topography in the study areas, and the directions of dune-forming winds are dominantly controlled by deflection and funneling at these local scales.

Assuming the ancient dunes migrated at rates similar to modern barchans (e.g., between 0.7 m/Mars year; Silvestro et al., 2013; and ~10 m/Mars year; Silvestro et al., 2010), it would take more than one Martian

season to align the dunes to a new wind direction. We therefore reject the interpretation that strong winds persisted from multiple directions over seasonal time scales. Instead, the paleodune orientation is representative of the long-term winds.

The size of the ancient dunes can also be inferred from the differences between modern dune and modeled pit measurements at Oyama and Herschel craters. In the modeled pits, the mean length and width decreased from the modern measurements by ~30%. The modeled pits are of similar size to the pits studied in this work, and the stoss and lee slopes on modern and ancient dunes are presumed to be the same to within a degree or two (Silvestro et al., 2013). Thus, we interpret that the above scaling relationship can be backward applied to the studied Martian pits to infer mean dune sizes in the partially buried ancient field. In the Hellas basin, a mean width of 402 m and mean length of 327 m translate to ancient dunes averaging 574 and 467 m in width and length, respectively. In Noctis Labyrinthus, a mean width of 136 m and mean length of 177 m translate to ancient dunes with mean widths and lengths of 194 and 253 m, respectively.

The above 30% scaling relationship applies because the modeled pits and those studied on Mars are similar in size. More generally, we can estimate the amount of apparent size reduction from dune to pit in the length direction by assuming a stoss slope of $\theta = 12°$ and a lee slope of $\phi = 30°$. In this case, the size reduction, dx, in the length direction is given simply by the sum of the portions of lee and stoss slopes that are covered, which is a function of the burial depth z. In other words, we can estimate the size reduction as

$$\mathbf{d}x = \frac{z}{\tan(\theta)} + \frac{z}{\tan(\phi)}.$$

By plugging in the 6-m depth used in modeling the pits, we can estimate a theoretical size reduction of ~38 m in the length direction for both the Oyama and Herschel crater modeled pits. This theoretical value matches well with the decrease in mean length seen in Oyama model pits (~37 m) but less well with the reduction seen in Herschel modeling (85 m). This difference could be attributed to an overestimate of the stoss and lee slopes in Herschel crater.

Preserved strata seen in ghost dune pits on Earth (Gaylord et al., 2016) suggest that strata may also be present in the Martian ghost dune pits. However, the extent to which some of the paleodune strata may be preserved in the pit interiors cannot be determined from orbit. Recent identification of an eolian sandstone in Gale crater by the rover *Curiosity* demonstrated how an eolian sandstone clearly exposed at the surface could not be identified as such from even HiRISE orbital images (Banham et al., 2018). At the locations studied in this work, identification of eolian strata is further complicated by the expected location of any strata to be on the pit floors, where modern eolian sands obscure the surface, or near the pit walls, where surfaces are shadowed and have unfavorable viewing geometries. Nevertheless, the dune cast formation mechanism proposed in this work suggests that some preservation of the ancient dune strata is likely (Figure 7). As discussed above (section 5.2), we favor a basalt flow or fluviolacustrine mechanism for the partial burial of the dunes. In either of these cases, cementation of the dune strata could occur at the interface between dune and burying material by interaction with melt or liquid water.

Preserved eolian strata in pits may be targets of interest for potential astrobiological preservation. Dunes have been proposed as potential refugia for Martian life (Fisk et al., 2013; Kereszturi et al., 2012) and are known to harbor life on Earth (Li et al., 2015). Modern eolian sediments on Mars have been shown to have adsorbed water on grain surfaces (Ehlmann et al., 2017; Leshin et al., 2013), and the frequent mixing of active sands would provide microbial life with a replenishing nutrient source (Fisk et al., 2013). Dune sands would further have protected early life from surface radiation. Preserved deposits from the paleodunes interpreted in this study (white arrows in Figure 7f) would be of particular interest to astrobiology, because (1) the strata have been protected from ionizing radiation by the overlying or surrounding smooth deposit, (2) the strata formed at an interface with a differing geologic material, creating a chemical gradient across the two, (3) a fluviolacustrine deposition would imply the strata were cemented in the presence of liquid water, and (4) a basalt deposition interpretation would imply the strata reflect an environment that was, at one time, locally warm.

6. Conclusions

The fields of pits studied in Noctis Labyrinthus and Hellas basin formed from partial burial of an eolian dune field, subsequent induration of the flood material, and later erosion of the uncemented dune sands, as shown

schematically in Figure 7. Basalt flows or subaqueous sedimentation are the most likely mechanisms for partial burial of the paleodunes. Comparisons of pit morphology and scale with modern Martian dunes and modeled pits support the above interpretation and provide a preponderance of evidence that the studied pits preserve eolian dune forms and are analogous to ghost dune pits seen on Earth. Synthetic pits modeled after modern dunes show a ~30% decrease in size from dune to pit, reflecting the tapering vertical profile of dunes in general. From this relationship, we infer that the paleodunes in Noctis Labyrinthus had mean lengths of ~250 m and in Hellas basin had mean lengths of ~470 m. The paleodunes in the two pit fields both record northerly paleowinds that differ from the current local Martian wind regime and reflect either a change in the climate or local dominance of topographic funneling of winds. The studied pits are also proposed as potential targets of astrobiological interest, because paleodune strata may be preserved along the pit margins. Although they are not visible from orbit, preserved strata in the pits would have become cemented at the interface with the burying material, which, depending on the mechanism, may have provided liquid water, warm temperatures, and a geochemical gradient. Preserved strata from the margins of the paleodunes would be protected from damaging radiation by the overlying burying deposit and therefore provide the potential for ancient biosignature preservation.

Acknowledgments
The authors thank J. Bourgeois, G. Kocurek, J. Levy, S. Sholes, and T. Goudge for helpful discussion regarding this work and thank D. Gaylord and M. Lapotre for their helpful reviews. Funding was provided through the NASA Postdoctoral Program, plus a NASA Habitable Worlds grant NNX15AP19G awarded to DCC. Image data used are listed in the figure captions and section 3. Data tables of dune and pit measurements are archived in a Github repository at https://github.com/GALE-Lab/Day2018_JGRPlanets_GhostDuneData.

References

Ahlbrandt, T. S., & Fryberger, S. G. (1981). Sedimentary features and significance of interdune deposits.
Allen, J. (1968). Flute marks and flute separation. *Nature*, *219*(5154), 602–604. https://doi.org/10.1038/219602a0
Allen, J. (1976). Computational models for dune time-lag: General ideas, difficulties, and early results. *Sedimentary Geology*, *15*(1), 1–53. https://doi.org/10.1016/0037-0738(76)90020-8
Baker, V. R. (2009). The channeled scabland: A retrospective. *Annual Review of Earth and Planetary Sciences*, *37*(1), 393–411. https://doi.org/10.1146/annurev.earth.061008.134726
Baker, V. R., & Milton, D. J. (1974). Erosion by catastrophic flooding on Mars and Earth. *Icarus*, *23*(1), 27–41. https://doi.org/10.1016/0019-1035(74)90101-8
Bandfield, J. L., Edgett, K. S., & Christensen, P. R. (2002). Spectroscopic study of the Moses Lake dune field, Washington: Determination of compositional distributions and source lithologies. *Journal of Geophysical Research*, *107*(E11), 5092. https://doi.org/10.1029/2000JE001469
Banham, S. G., Gupta, S., Rubin, D. M., Watkins, J. A., Sumner, D. Y., Edgett, K. S., et al. (2018). Ancient Martian aeolian processes and palaeomorphology reconstructed from the Stimson formation on the lower slope of Aeolis Mons, Gale crater, Mars. *Sedimentology*, *65*, 993–1042. https://doi.org/10.1111/sed.12469
Benan, C. A. A., & Kocurek, G. (2000). Catastrophic flooding of an aeolian dune field: Jurassic Entrada and Todilto Formations, Ghost Ranch, New Mexico, USA. *Sedimentology*, *47*(6), 1069–1080. https://doi.org/10.1046/j.1365-3091.2000.00341.x
Bourke, M., & Viles, H. (2016). Valley floor aeolianite in an equatorial pit crater on Mars. *Geophysical Research Letters*, *43*, 12,356–12,362. https://doi.org/10.1002/2016GL071467
Bourke, M. C. (2010). Barchan dune asymmetry: Observations from Mars and Earth. *Icarus*, *205*(1), 183–197. https://doi.org/10.1016/j.icarus.2009.08.023
Bourke, M. C., Balme, M., Beyer, R. A., Williams, K. K., & Zimbelman, J. (2006). A comparison of methods used to estimate the height of sand dunes on Mars. *Geomorphology*, *81*(3), 440–452.
Bridges, N. T., Kocurek, G. A., Langevin, Y., Lewis, K. W., Mangold, N., Maurice, S., et al. (2014). The rock abrasion record at Gale Crater: Mars Science Laboratory results from Bradbury Landing to Rocknest. *Journal of Geophysical Research: Planets*, *119*, 1374–1389. https://doi.org/10.1002/2013JE004579
Bristow, C., & Hill, N. (1998). Dune morphology and palaeowinds from aeolian sandstones in the Miocene Shuwaihat Formation, Abu Dhabi, United Arab Emirates. In A. S. Alsharhan, et al. (Eds.), *Proceedings International Conference on Quaternary Deserts and Climate Change* (pp. 553–564).
Brookfield, M. (1977). The origin of bounding surfaces in ancient aeolian sandstones. *Sedimentology*, *24*(3), 303–332. https://doi.org/10.1111/j.1365-3091.1977.tb00126.x
Brothers, S. C., Kocurek, G., Brothers, T. C., & Buynevich, I. (2016). Stratigraphic architecture resulting from dune interactions: White Sands Dune Field, New Mexico. *Sedimentology*. https://doi.org/10.1111/sed.%2012320
Brothers, S. C., Kocurek, G., & Holt, J. W. (2018). Sequence architecture of the cavi unit, Chasma Boreale, Mars. *Icarus*, *308*, 42–60. https://doi.org/10.1016/j.icarus.2017.06.024
Carr, M. H. (1974). Tectonism and volcanism of the Tharsis region of Mars. *Journal of Geophysical Research*, *79*(26), 3943–3949. https://doi.org/10.1029/JB079i026p03943
Carr, M. H. (1982). Periodic climate change on Mars: Review of evidence and effects on distribution of volatiles. *Icarus*, *50*(2), 129–139.
Carr, M. H. (2001). Mars Global Surveyor observations of Martian fretted terrain. *Journal of Geophysical Research*, *106*(E10), 23,571–23,593. https://doi.org/10.1029/2000JE001316
Catling, D. C., Wood, S. E., Leovy, C., Montgomery, D. R., Greenberg, H. M., Glein, C. R., & Moore, J. M. (2006). Light-toned layered deposits in Juventae Chasma, Mars. *Icarus*, *181*(1), 26–51. https://doi.org/10.1016/j.icarus.2005.10.020
Christensen, P. R., Bandfield, J. L., Bell, J. F. III, Gorelick, N., Hamilton, V. E., Ivanov, A., et al. (2003). Morphology and composition of the surface of Mars: Mars Odyssey THEMIS results. *Science*, *300*(5628), 2056–2061. https://doi.org/10.1126/science.1080885
Courrech du Pont, S., Narteau, C., & Gao, X. (2014). Two modes for dune orientation. *Geology*, *42*(9), 743–746. https://doi.org/10.1130/G35657.1
Crown, D. A., Bleamaster, L. F., & Mest, S. C. (2005). Styles and timing of volatile-driven activity in the eastern Hellas region of Mars. *Journal of Geophysical Research*, *110*, E12S22. https://doi.org/10.1029/2005JE002496
Crown, D. A., & Greeley, R. (1993). Volcanic geology of Hadriaca Patera and the eastern Hellas region of Mars. *Journal of Geophysical Research*, *98*(E2), 3431–3451. https://doi.org/10.1029/92JE02804

Crown, D. A., & Greeley, R. (2007). Geologic map of the MTM-30262 and-30267 quadrangles, Hadriaca Patera region of Mars: Geological Survey (US), 2329-132X.
Crown, D. A., Price, K. H., & Greeley, R. (1992). Geologic evolution of the east rim of the Hellas basin Mars. *Icarus*, *100*(1), 1–25. https://doi.org/10.1016/0019-1035(92)90014-X
Day, M., Anderson, W., Kocurek, G., & Mohrig, D. (2016). Carving intracrater layered deposits with wind on Mars. *Geophysical Research Letters*, *43*, 2473–2479. https://doi.org/10.1002/2016GL068011
Day, M., & Kocurek, G. (2016). Observations of an aeolian landscape: From surface to orbit in Gale Crater. *Icarus*, *280*, 37–71. https://doi.org/10.1016/j.icarus.2015.09.042
Day, M., & Kocurek, G. (2017). Aeolian dune interactions preserved in the ancient rock record. *Sedimentary Geology*, *358*, 187–196. https://doi.org/10.1016/j.sedgeo.2017.07.009
Durand, A. (1982). Oscillations of Lake Chad over the past 50,000 years: New data and new hypothesis. *Palaeogeography, Palaeoclimatology, Palaeoecology*, *39*(1–2), 37–53. https://doi.org/10.1016/0031-0182(82)90071-2
Edgett, K., & Malin, M. (2000). Examples of Martian sandstone: Indurated, lithified, and cratered eolian dunes in MGS MOC images. In Proceedings 31st Lunar and Planetary Science Conference, Houston, TX, Abstract 1071.
Edgett, K. S., & Blumberg, D. G. (1994). Star and linear dunes on Mars. *Icarus*, *112*(2), 448–464. https://doi.org/10.1006/icar.1994.1197
Edgett, K. S., & Lancaster, N. (1993). Volcaniclastic aeolian dunes: Terrestrial examples and application to Martian sands. *Journal of Arid Environments*, *25*(3), 271–297. https://doi.org/10.1006/jare.1993.1061
Edwards, C. S., Bandfield, J. L., Christensen, P. R., & Fergason, R. L. (2009). Global distribution of bedrock exposures on Mars using THEMIS high-resolution thermal inertia. *Journal of Geophysical Research*, *114*, E11001. https://doi.org/10.1029/2009JE003363
Ehlmann, B. L., Edgett, K. S., Sutter, B., Achilles, C. N., Litvak, M. L., Lapotre, M. G., et al. (2017). Chemistry, mineralogy, and grain properties at Namib and High dunes, Bagnold dune field, Gale crater, Mars: A synthesis of Curiosity rover observations. *Journal of Geophysical Research: Planets*, *122*, 2510–2543. https://doi.org/10.1002/2017JE005267
Ewing, R. C., & Kocurek, G. (2010). Aeolian dune interactions and dune-field pattern formation: White Sands Dune Field, New Mexico. *Sedimentology*, *57*(5), 1199–1219.
Ewing, R. C., Kocurek, G., & Lake, L. W. (2006). Pattern analysis of dune-field parameters. *Earth Surface Processes and Landforms*, *31*(9), 1176–1191. https://doi.org/10.1002/esp.1312
Ewing, R. C., Lapotre, M. G. A., Lewis, K. W., Day, M., Stein, N., Rubin, D. M., et al. (2017). Sedimentary processes of the Bagnold Dunes: Implications for the eolian rock record of Mars. *Journal of Geophysical Research: Planets*, *122*, 2544–2573. https://doi.org/10.1002/2017JE005324
Fenton, L. K., & Hayward, R. K. (2010). Southern high latitude dune fields on Mars: Morphology, aeolian inactivity, and climate change. *Geomorphology*, *121*(1), 98–121.
Fergason, R. L., Christensen, P. R., & Kieffer, H. H. (2006). High-resolution thermal inertia derived from the Thermal Emission Imaging System (THEMIS): Thermal model and applications. *Journal of Geophysical Research*, *111*, E12004. https://doi.org/10.1029/2006JE002735
Fisk, M., Popa, R., Bridges, N., Renno, N., Mischna, M., Moores, J., & Wiens, R. (2013). Habitability of transgressing Mars dunes. *Geochimica et Cosmochimica Acta*, *67*, 3871–3887.
Forget, F., Hourdin, F., Fournier, R., Hourdin, C., Talagrand, O., Collins, M., et al. (1999). Improved general circulation models of the Martian atmosphere from the surface to above 80 km. *Journal of Geophysical Research*, *104*(E10), 24,155–24,175. https://doi.org/10.1029/1999JE001025
Gao, X., Narteau, C., Rozier, O., & du Pont, S. C. (2015). Phase diagrams of dune shape and orientation depending on sand availability. *Scientific Reports*, *5*, 14677.
Gaylord, D. R., Link, P. K., & McKoon, J. T. (2015). Provenance of the Pleistocene and Holocene St. Anthony Dune Field, Eastern Snake River Plain, Idaho: Insights from U/Pb detrital zircon geochronology. *Northwest Geology – The Journal of the Tobacco Toon Geological Society*, *44*, 89–100.
Gaylord, D. R., Link, P. K., & Ruittenour, T. M. (2016). Geological field guide to the Holocene northeastern St. Anthony dune field and mid-late pleistocene ghost dunes, Eastern Snake River Plain, Idaho. *Northwest Geology – The Journal of the Tobacco Toon Geological Society*, *45*, 85–94.
Glamoclija, M., Marinangeli, L., & Komatsu, G. (2011). Harmakhis Vallis source region, Mars: Insights into the recent geothermal history based on geological mapping. *Planetary and Space Science*, *59*(11), 1179–1194.
Greeley, R., Kuzmin, R. O., & Haberle, R. M. (2001). Aeolian processes and their effects on understanding the chronology of Mars. *Space Science Reviews*, *96*(1), 393–404.
Grotzinger, J. P., Arvidson, R. E., Bell, J. F., Calvin, W., Clark, B. C., Fike, D. A., et al. (2005). Stratigraphy and sedimentology of a dry to wet eolian depositional system, Burns formation, Meridiani Planum, Mars. *Earth and Planetary Science Letters*, *240*(1), 11–72. https://doi.org/10.1016/j.epsl.2005.09.039
Hayward, R. K., Fenton, L. K., & Titus, T. N. (2014). Mars Global Digital Dune Database (MGD(3)): Global dune distribution and wind pattern observations. *Icarus*, *230*, 38–46. https://doi.org/10.1016/j.icarus.2013.04.011
Hersen, P. (2004). On the crescentic shape of barchan dunes. *The European Physical Journal B*, *37*(4), 507–514. https://doi.org/10.1140/epjb/e2004-00087-y
Hunter, R. (1976). Comparison of eolian and subaqueous sand-flow cross-strata. In Proceedings AAPG-SEPM Annual Meeting, Volume 60, p. 683–684, Abstract 90972.
Jerram, D. A., Mountney, N. P., Howell, J. A., Long, D., & Stollhofen, H. (2000). Death of a sand sea: An active aeolian erg systematically buried by the Etendeka flood basalts of NW Namibia. *Journal of the Geological Society*, *157*(3), 513–516. https://doi.org/10.1144/jgs.157.3.513
Kadish, S. J., Head, J. W., Barlow, N. G., & Marchant, D. R. (2008). Martian pedestal craters: Marginal sublimation pits implicate a climate-related formation mechanism. *Geophysical Research Letters*, *35*, L16104. https://doi.org/10.1029/2008GL034990
Kereszturi, Á., Bérczi, S., Horváth, A., Pócs, T., Sik, A., & Eörs, S. (2012). The astrobiological potential of polar dunes on Mars. In A. Hanslmeier, S. Kempe, & J. Seckbach (Eds.), *Life on Earth and other Planetary Bodies*. Cellular Origin, Life in Extreme Habitats and Astrobiology (Vol 24). Dordrecht, Netherlands: Springer. https://doi.org/10.1007/978-94-007-4966-5_25
Kocurek, G., & Day, M. (2017). What is preserved in the aeolian rock record? A Jurassic Entrada Sandstone case study at the Utah-Arizona border. *Sedimentology*, *65*, 1301–1321. https://doi.org/10.1111/sed.12422
Kocurek, G., & Ewing, R. C. (2005). Aeolian dune field self-organization—Implications for the formation of simple versus complex dune-field patterns. *Geomorphology*, *72*(1–4), 94–105. https://doi.org/10.1016/j.geomorph.2005.05.005
Kocurek, G., & Ewing, R. C. (2012). Source-to-sink: An Earth/Mars comparison of boundary conditions for eolian dune systems. In *Sedimentary geology of Mars* (pp. 151–168). SEPM Special Publication No. 102, Tulsa, OK.

Kocurek, G., Ewing, R. C., & Mohrig, D. (2010). How do bedform patterns arise? New views on the role of bedform interactions within a set of boundary conditions. *Earth Surface Processes and Landforms*, *35*(1), 51–63. https://doi.org/10.1002/esp.1913

Kocurek, G., & Lancaster, N. (1999). Aeolian system sediment state: Theory and Mojave Desert Kelso dune field example. *Sedimentology*, *46*(3), 505–515. https://doi.org/10.1046/j.1365-3091.1999.00227.x

Kuntz, M. A., Covington, H. R., & Schorr, L. J. (1992). An overview of basaltic volcanism of the eastern Snake River Plain, Idaho. Regional Geology of Eastern Idaho and Western Wyoming. *Geological Society of America Memoirs*, *179*, 227–267. https://doi.org/10.1130/MEM179-p227

Laity, J. E. (1994). Landforms of aeolian erosion. In A. D. Abrahams & A. J. Parsons (Eds.), *Geomorphology of desert environments* (pp. 506–535). Dordrecht: Springer Netherlands. https://doi.org/10.1007/978-94-015-8254-4_19

Lamb, M. P., & Mohrig, D. (2009). Do hyperpycnal-flow deposits record river-flood dynamics? *Geology*, *37*(12), 1067–1070. https://doi.org/10.1130/G30286A.1

Lapotre, M. G. A., Ewing, R. C., Lamb, M. P., Fischer, W. W., Grotzinger, J. P., Rubin, D. M., et al. (2016). Large wind ripples on Mars: A record of atmospheric evolution. *Science*, *353*(6294), 55–58. https://doi.org/10.1126/science.aaf3206

Leshin, L. A., Mahaffy, P. R., Webster, C. R., Cabane, M., Coll, P., Conrad, P. G., et al. (2013). Volatile, isotope, and organic analysis of Martian fines with the Mars curiosity rover. *Science*, *341*(6153), 1238937.

Li, K., Bai, Z., & Zhang, H. (2015). Community succession of bacteria and eukaryotes in dune ecosystems of Gurbantünggüt Desert, Northwest China. *Extremophiles*, *19*(1), 171–181. https://doi.org/10.1007/s00792-014-0696-z

Loope, D. B., & Rowe, C. M. (2003). Long-lived pluvial episodes during deposition of the Navajo sandstone. *The Journal of Geology*, *111*(2), 223–232. https://doi.org/10.1086/345843

Lorenz, R., Fenton, L., & Lancaster, N. (2015). The tallest dunes in the solar system? Dune heights on Earth, Mars, Titan and Venus. In Proceedings Fourth Annual International Planetary Dunes Workshop, Volume 1843, Abstract 8031.

Malin, M. C., Bell, J. F., Cantor, B. A., Caplinger, M. A., Calvin, W. M., Clancy, R. T., et al. (2007). Context camera investigation on board the Mars Reconnaissance Orbiter. *Journal of Geophysical Research*, *112*, E05S04. https://doi.org/10.1029/2006JE002808

Mangold, N., Roach, L., Milliken, R., Le Mouélic, S., Ansan, V., Bibring, J., et al. (2010). A Late Amazonian alteration layer related to local volcanism on Mars. *Icarus*, *207*(1), 265–276. https://doi.org/10.1016/j.icarus.2009.10.015

Masson, P. (1977). Structure pattern analysis of the Noctis Labyrinthus-Valles Marineris regions of Mars. *Icarus*, *30*(1), 49–62. https://doi.org/10.1016/0019-1035(77)90120-8

McEwen, A. S., Eliason, E. M., Bergstrom, J. W., Bridges, N. T., Hansen, C. J., Delamere, W. A., et al. (2007). Mars reconnaissance Orbiter's High Resolution Imaging Science Experiment (HiRISE). *Journal of Geophysical Research*, *112*, E05S02. https://doi.org/10.1029/2005JE002605

Milliken, R. E., Ewing, R. C., Fischer, W. W., & Hurowitz, J. (2014). Wind-blown sandstones cemented by sulfate and clay minerals in Gale Crater, Mars. *Geophysical Research Letters*, *41*, 1149–1154. https://doi.org/10.1002/2013GL059097

Millour, E., Forget, F., Spiga, A., Navarro, T., Madeleine, J.-B., Montabone, L., et al. (2015). The Mars Climate Database (MCD version 5.2) European Planetary Science Congress Volume 10.

Mulder, T., Syvitski, J. P., Migeon, S., Faugeres, J.-C., & Savoye, B. (2003). Marine hyperpycnal flows: Initiation, behavior and related deposits. A review. *Marine and Petroleum Geology*, *20*(6–8), 861–882. https://doi.org/10.1016/j.marpetgeo.2003.01.003

Normark, W. R., Paull, C. K., Caress, D. W., Ussler, W. III, & Sliter, R. (2009). Fine-scale relief related to Late Holocene channel shifting within the floor of the upper Redondo Fan, offshore Southern California. *Sedimentology*, *56*(6), 1690–1704. https://doi.org/10.1111/j.1365-3091.2009.01052.x

Parteli, E. J. R., Duran, O., Bourke, M. C., Tsoar, H., Poschel, T., & Herrmann, H. (2014). Origins of barchan dune asymmetry: Insights from numerical simulations. *Aeolian Research*, *12*, 121–133. https://doi.org/10.1016/j.aeolia.2013.12.002

Peterfreund, A. R. (1985). Contemporary aeolian processes on Mars: Local dust storms. *Dissertation*. PhD. Arizona State University, Tempe, AZ.

Petrone, A. (1970). The Moses Lake sand dunes. *Thesis*. M.S.: Washington State University, Pulman, WA.

Price, K. H. (1998). Geologic map of the Dao, Harmakhis, and Reull Valles region of Mars, US Geological Survey, Information Services. I-2557, scale 1:1,000,000.

Robertson, E. C. (1988). Thermal properties of rocks: US Geological Survey, 2331-1258.

Rodriguez, J. A. P., Zarroca, M., Linares, R., Gulick, V., Weitz, C. M., Yan, J., et al. (2016). Groundwater flow induced collapse and flooding in Noctis Labyrinthus, Mars. *Planetary and Space Science*, *124*, 1–14.

Rubin, D. M., & Hunter, R. E. (1987). Bedform alignment in directionally varying flows. *Science*, *237*(4812), 276–278. https://doi.org/10.1126/science.237.4812.276

Schatz, V., Tsoar, H., Edgett, K. S., Parteli, E. J. R., & Herrmann, H. J. (2006). Evidence for indurated sand dunes in the Martian north polar region. *Journal of Geophysical Research*, *111*, E04006. https://doi.org/10.1029/2005JE002514

Scott, D. H., & Tanaka, K. L. (1986). Geologic map of the western equatorial region of Mars: US Geological Survey. Map I-1802-A, scale 1:15,000,000.

Sharp, R. P. (1973). Mars: Fretted and chaotic terrains. *Journal of Geophysical Research*, *78*(20), 4073–4083. https://doi.org/10.1029/JB078i020p04073

Shean, D. E., Alexandrov, O., Moratto, Z. M., Smith, B. E., Joughin, I. R., Porter, C., & Morin, P. (2016). An automated, open-source pipeline for mass production of digital elevation models (DEMs) from very-high-resolution commercial stereo satellite imagery. *ISPRS Journal of Photogrammetry and Remote Sensing*, *116*, 101–117. https://doi.org/10.1016/j.isprsjprs.2016.03.012

Sides, S., Becker, T., Becker, K., Edmundson, K., Backer, J., Wilson, T., et al. (2017). The USGS Integrated Software for Imagers and Spectrometers (ISIS 3) Instrument Support, New Capabilities, and Releases. In Proceedings Lunar and Planetary Science Conference, Volume 48.

Silvestro, S., Fenton, L. K., Vaz, D. A., Bridges, N. T., & Ori, G. G. (2010). Ripple migration and dune activity on Mars: Evidence for dynamic wind processes. *Geophysical Research Letters*, *37*, L20203. https://doi.org/10.1029/2010GL044743

Silvestro, S., Vaz, D. A., Ewing, R. C., Rossi, A. P., Fenton, L. K., Michaels, T. I., et al. (2013). Pervasive aeolian activity along rover Curiosity's traverse in Gale Crater, Mars. *Geology*, *41*(4), 483–486. https://doi.org/10.1130/G34162.1

Spencer, J. R., & Fanale, F. P. (1990). New models for the origin of Valles Marineris closed depressions. *Journal of Geophysical Research*, *95*(B9), 14,301–14,313. https://doi.org/10.1029/JB095iB09p14301

Steele, L. J., Kite, E. S., & Michaels, T. I. (2018). Crater mound formation by wind erosion on Mars. *Journal of Geophysical Research: Planets*, *123*, 113–130. https://doi.org/10.1002/2017JE005459

Tanaka, K. L., & Leonard, G. J. (1995). Geology and landscape evolution of the Hellas region of Mars. *Journal of Geophysical Research*, *100*(E3), 5407–5432. https://doi.org/10.1029/94JE02804

Tanaka, K. L., Skinner, J. A. Jr., Dohm, J. M., Irwin, R. P. III, Kolb, E. J., Fortezzo, C. M., et al. (2014). Geologic map of Mars, scale 1:20,000,000, Pamphlet 43 P.

Waichel, B. L., Scherer, C. M. S., & Frank, H. T. (2008). Basaltic lava flows covering active aeolian dunes in the Paraná Basin in southern Brazil: Features and emplacement aspects. *Journal of Volcanology and Geothermal Research*, *171*(1), 59–72.

Ward, A. W. (1979). Yardangs on Mars—Evidence of recent wind erosion. *Journal of Geophysical Research*, *84*(B14), 8147–8166. https://doi.org/10.1029/JB084iB14p08147

Weitz, C. M., Bishop, J. L., Thollot, P., Mangold, N., & Roach, L. H. (2011). Diverse mineralogies in two troughs of Noctis Labyrinthus, Mars. *Geology*, *39*(10), 899–902. https://doi.org/10.1130/G32045.1

Werner, B. T., & Kocurek, G. (1999). Bedform spacing from defect dynamics. *Geology*, *27*(8), 727–730. https://doi.org/10.1130/0091-7613(1999)027%3C0727:BSFDD%3E2.3.CO;2

Williams, D. A., Greeley, R., Zuschneid, W., Werner, S. C., Neukum, G., Crown, D. A., et al. (2007). Hadriaca Patera: Insights into its volcanic history from Mars Express High Resolution Stereo Camera. *Journal of Geophysical Research*, *112*, E10004. https://doi.org/10.1029/2007JE002924

Worman, S. L., Murray, A. B., Littlewood, R., Andreotti, B., & Claudin, P. (2013). Modeling emergent large-scale structures of barchan dune fields. *Geology*, *41*(10), 1059–1062. https://doi.org/10.1130/G34482.1

Wyrick, D., Ferrill, D. A., Morris, A. P., Colton, S. L., & Sims, D. W. (2004). Distribution, morphology, and origins of Martian pit crater chains. *Journal of Geophysical Research*, *109*, E06005. https://doi.org/10.1029/2004JE002240